Projected Changes in South Asian Monsoon Low Pressure Systems

WENHAO DONG

Geophysical Fluid Dynamics Laboratory/NOAA, Princeton, New Jersey, and Cooperative Programs for the Advancement of Earth System Science, University Corporation for Atmospheric Research, Boulder, Colorado

YI MING AND V. RAMASWAMY

Geophysical Fluid Dynamics Laboratory/NOAA, Princeton, New Jersey

(Manuscript received 11 March 2020, in final form 8 June 2020)

ABSTRACT

Monsoon low pressure systems (MLPSs) are among the most important synoptic-scale disturbances of the South Asian summer monsoon. Potential changes in their characteristics in a warmer climate would have broad societal impacts. Yet, the findings from a few existing studies are inconclusive. We use the Geophysical Fluid Dynamics Laboratory (GFDL) coupled climate model CM4.0 to examine the projected changes in the simulated MLPS activity under a future emission scenario. It is shown that CM4.0 can skillfully simulate the number, genesis location, intensity, and lifetime of MLPSs. Global warming gives rise to a significant decrease in MLPS activity. An analysis of several large-scale environmental variables, both dynamic and thermodynamic, suggests that the decrease in MLPS activity can be attributed mainly to a reduction in low-level relative vorticity over the core genesis region. The decreased vorticity is consistent with weaker large-scale ascent, which leads to less vorticity production through the stretching term in the vorticity equation. Assuming a fixed radius of influence, the projected reduction in MLPSs would significantly lower the associated precipitation over north-central India, despite an overall increase in mean precipitation.

1. Introduction

Cyclonic vortices of varying intensity, collectively known as monsoon low pressure systems (MLPSs), are an important feature of the South Asian summer monsoon (Sikka 2006; Yoon and Huang 2012; Hurley and Boos 2015; Hunt et al. 2016a; Adames and Ming 2018a,b; Clark et al. 2020). Occurring within the large-scale monsoon trough, MLPSs are the primary rain-producing synoptic-scale systems over the Indian subcontinent, and are estimated to be responsible for more than half of the annual precipitation in agrarian northern and central India (Ding and Sikka 2006; Krishnamurthy and Ajayamohan 2010). These transient disturbances typically travel westward or northwestward across the subcontinent after formation, transporting large amounts of moisture from the Bay of Bengal (BoB). Changes in the characteristics of MLPSs, whether natural or forced, would have far-reaching socioeconomical impacts. For instance, the anomalously large number of MLPSs in 2006 resulted in excess rainfall over central India, leading to widespread flooding and damage (Jayanthi et al. 2006; Krishnan et al. 2011).

Understanding future changes in MLPSs and associated rainfall is a necessary step toward projecting flood or drought risks in a warmer climate. To date, only a few studies have investigated potential changes in South Asian MLPSs, without conclusive findings (Stowasser et al. 2009; Rastogi et al. 2018; Sandeep et al. 2018). There are at least two hindering factors. First, MLPSs are relatively weak (especially compared to tropical cyclones), making it difficult to devise effective tracking algorithms (Praveen et al. 2015). Earlier studies of MLPS tracks were based mainly on manual evaluation of meteorological pressure charts (Mooley and Shukla 1988; Sikka 2006; Prajeesh et al. 2013). Following the advent of satellite and reanalysis datasets with global

Denotes content that is immediately available upon publication as open access.

Corresponding author: Wenhao Dong, wenhao.dong@noaa.gov

Publisher's Note: This article was revised on 17 March 2021 to update the manuscript received date, which had the incorrect year when originally published.

DOI: 10.1175/JCLI-D-20-0168.1

coverage, the reliability of these analyses was called into question over inconsistencies among different datasets, particularly over ocean (Cohen and Boos 2014; Hurley and Boos 2015). This led to the development of several automated MLPS tracking algorithms in recent years (Hurley and Boos 2015; Praveen et al. 2015; Hunt et al. 2016a). Second, the generally poor representation of MLPSs in global climate model (GCM) simulations erodes the confidence in future projections. By applying the automated algorithms to model outputs, one can show that although most GCMs are able to capture the basic structure of MLPSs, they are deficient in reproducing the occurrence frequency and tracks (Praveen et al. 2015; Rastogi et al. 2018). This is true for the majority of models from phase 5 of the Coupled Model Intercomparison Project (CMIP5), which show no significant changes in either the occurrence frequency or tracks of MLPSs in the twenty-first century under the RCP8.5 scenario (Rastogi et al. 2018). These results, however, are at odds with Sandeep et al. (2018) based on a 50-km atmospheric model (HiRAM) developed at the Geophysical Fluid Dynamics Laboratory (GFDL) (Zhao et al. 2009), which is more skillful at simulating MLPSs than CMIP models. This model projects a significant decrease and poleward shift in MLPS activity. HiRAM, however, substantially overestimates the density track of MLPSs and, contrary to observations, simulates more genesis over land than over ocean. It is unclear how these biases may skew future projection.

Although it is difficult to compare the existing studies objectively due to discrepancies in tracking methods and model setups, the lack of consensus highlights the need for robust quantitative assessment of the projected changes in MLPSs using the latest tracking algorithms and GCMs. In this study, we employ the state-of-the-art climate model GFDL CM4.0 (one of the CMIP6 models) to investigate how the model-simulated MLPSs would vary in a warmer climate. Fully coupled simulations, rather than atmosphere-only simulations forced with prescribed sea surface temperatures (SSTs) and sea ice, are used in this study. This choice is justified by the consideration that atmosphere-only simulations such as those used in Sandeep et al. (2018) cannot fully represent the impacts of changes in surface fluxes and oceanic mixed layer depth, potentially leading to unrealistic results (Praveen et al. 2015). These issues are particularly acute over the South Asian monsoon region, where the air–sea coupling is strong (Lau and Nath 2003). Our work demonstrates that CM4.0 can skillfully simulate the key characteristics of MLPSs (e.g., number, genesis location, intensity, and lifetime). Furthermore, CM4.0 projects a persistent decrease in the number of MLPSs throughout the twenty-first century, which is attributed primarily to reduced low-level relative vorticity over the core genesis region. Less frequent synoptic disturbances lead to a significant decrease in MLPS-related precipitation over north-central India.

2. Methodology

a. Observational data

The 6-hourly ERA-Interim data at a horizontal resolution of 0.7° (Dee et al. 2011) are used to identify MLPSs during the monsoon season (June–September) for 1979–2018. An automated tracking algorithm (detailed in section 2b) is applied to low-level relative vorticity, mean sea level pressure, and surface winds to track and classify MLPSs. A set of large-scale environmental variables (including vertical wind shear, midlevel relative humidity, total column water vapor, convective instability, and SST) are examined as to their effects on MLPS formation (Ditchek et al. 2016). Vertical wind shear is defined as the magnitude of the difference in winds between 200 and 850 hPa. Convective available potential energy (CAPE) (a measure of convective instability) is calculated as the accumulated buoyancy from the level of free convection to the equilibrium level. Except for SST, all environmental variables are based on the ERA-Interim data. The NOAA High-Resolution (0.25° × 0.25°) Blended Analysis of Daily SST (Reynolds et al. 2007; https://psl.noaa.gov/data/gridded/data.noaa.oisst.v2.highres.html) for 1982–2018 and the Global Precipitation Climatology Product (GPCP) daily precipitation data (Huffman et al. 2001) at 1° × 1° resolution for 1997–2018 are also used. As explained in section 2c, the main analysis period is 1979–2014. The ERA-Interim data for the same period are used for comparing with the historical simulation. As the NOAA SST and GPCP datasets do not cover the entire period, any comparison involving them is done for the overlapping years.

b. GFDL CM4.0 model simulations

The latest GFDL coupled atmosphere–ocean model CM4.0 is described in Held et al. (2019). The atmospheric component AM4.0 features a horizontal resolution of ~1°, 33 vertical levels, a double-plume convective parameterization, simplified chemistry sufficient for simulating aerosols from emissions, and aerosol indirect effects (Zhao et al. 2018a,b). The ocean component OM4 is a configuration of MOM6 with a horizontal resolution of 0.25° and 75 levels in a hybrid pressure–isopycnal vertical coordinate (Adcroft et al. 2019). Both the historical simulation (1850–2014) and the future simulation (2015–99) under the SSP5–8.5 scenario (fossil-fueled development) (O'Neill et al. 2016) are analyzed. The former is based on

the mean of a three-member ensemble, and the latter is based on one single realization.

c. MLPS tracking algorithm

We adopt the tracking algorithm described in Hunt et al. (2016a), which, at a 6-hourly time step, searches for candidate systems with maximum 850-hPa relative vorticity exceeding a threshold value of $1 \times 10^{-5}\,s^{-1}$. Note that the vorticity field is spectrally truncated to T42 to suppress small-scale noise. The India Meteorological Department (IMD) definitions are used to classify each candidate system according to its intensity measured in surface wind speed and sea level pressure (Hurley and Boos 2015). For example, monsoon depressions are cyclonic vortices with peak surface wind speed of 8.5–$13.5\,m\,s^{-1}$ and sea level pressure minimum of 4–10 hPa below the surrounding region. Candidates not satisfying the wind threshold criterion or without a nearby synoptic-scale surface low (a negative sea level pressure anomaly relative to the 21-day average) are discarded. As the typical translation speed of MLPS is much less than $10\,m\,s^{-1}$ (Hunt et al. 2016a; Adames and Ming 2018b), vortices present in consecutive 6-hourly outputs are then connected provided that the central vortex location has not moved faster than $10\,m\,s^{-1}$. Results based on this method have been compared extensively with the IMD archives, and used successfully in previous works (Hunt et al. 2016a,b; Hunt and Fletcher 2019).

Among the identified candidate systems, we select only those lasting longer than 2 days with genesis locations east of 75°E and south of 30°N during the monsoon season. MLPSs, which reach the monsoon depression level or stronger at any point, are collectively referred to as monsoon depressions throughout their lifetime in the following analysis, while weaker ones that still meet the minimum criteria are referred to as monsoon lows. MLPS occurrence frequency is calculated as histogram of 6-hourly locations aggregated in $1° \times 1°$ grid boxes. It is possible for a MLPS to be counted more than once in a grid box. We use the same period of 1979–2014 (36 monsoon seasons) both for the ERA-Interim and for the historical simulation to evaluate the model's skill in simulating MLPSs. The historical simulation is compared with the period of 2064–99 (the same duration) in the future simulation to assess the projected changes.

d. Statistical analysis

The statistical significance of the difference in track density is evaluated using a bootstrapping approach. For the combined historical and future simulations, we perform a 1000-fold resampling of 36-yr segments with replacement. The 95% confidence intervals are computed from the resampled data. Two-tailed Student's t tests are used to evaluate the differences in the large-scale environmental variables between the historical and future simulations. Only those found to be statistically significant at the 95% confidence level after considering the false discovery rate (Wilks 2016) are highlighted. To assess the statistical significance of future changes in the environmental variables composited on MLPS events, we perform a 1000-fold resampling of each variable with replacement for the combined historical and future simulations.

3. Results

a. Historical simulation of MLPSs

We start by evaluating the characteristics of MLPSs in the historical simulation. ERA-Interim indicates an average of 8.3 MLPSs (with a standard deviation of 1.8) per season, typically consisting of around five depressions and four lows. In comparison, the historical simulation produces an average of 7.1 MLPSs per season (around four depressions and three lows) (Table 1). The occurrence (genesis) over land is less frequent than over ocean, averaged at 2.2 and 6.1 per season, respectively, in ERA-Interim. The same behavior holds in the historical simulation as well; the occurrence is 1.5 per season over land and 5.6 per season over ocean.

The observed and simulated MLPS track densities are compared in Fig. 1. In ERA-Interim, MLPSs are distributed broadly over the South Asian monsoon region spanning from the BoB to the north-central India. A distinct maximum is located over the BoB along the east coast of India (Cohen and Boos 2014; Hurley and Boos 2015), which constitutes the part of India most vulnerable to flooding. A large fraction of floods occurring in this region are associated with the passage of MLPSs (Ajayamohan et al. 2010; Yoon and Huang 2012). CM4.0 simulates the track density fairly well, albeit with a slight southward shift. Conceptually, track density depends both on genesis location and on trajectory. The latitudinal centroid of the genesis location in ERA-Interim (18.1°N) is considerably northward of that in in the historical simulation (16.5°N) (Table 1). By contrast, the model-simulated MLPS trajectories are similar to those in ERA-Interim (Fig. 2). The mean direction of westward-propagating MLPSs relative to the due north is 286.8° in ERA-Interim, and 284.0° in the historical simulation, which are rather similar. Thus, the equatorward bias in the model-simulated track density is primarily attributable to the different genesis locations. This could be further linked to a common model deficiency referred to as the "Philippines hotspot," which is thought to be sensitive to convective parameterizations (Zhao et al. 2018a,b). It has been argued that the tropical

TABLE 1. Key characteristics of MLPSs in the ERA-Interim and historical simulation and the differences between the historical and future simulations (with statistical significance at the 95% confidence level highlighted in boldface).

	ERA-Interim	Historical simulation	Future minus historical
Number of events	8.3	7.1	**−1.3**
Land genesis	2.2	1.5	0.1
Oceanic genesis	6.1	5.6	**−1.4**
Depressions	4.7	4.4	**−0.8**
Lows	3.6	2.7	**−0.5**
Lifetime (days)	5.1	4.7	−0.2
Land genesis	4.5	4.3	−0.6
Oceanic genesis	5.2	4.8	−0.1
Depressions	6.1	5.3	−0.4
Lows	3.8	3.7	−0.5
Oceanic fraction (%)	44.7	58.3	−4.2
Centroid of latitude (°N)	18.1	16.7	−0.5
Centroid of longitude (°E)	87.0	86.4	−0.0
Propagation heading (°)	286.8	284.0	−1.7

disturbance originating over the South China Sea or west Pacific could trigger MLPSs over the BoB (Krishnamurti et al. 1977; Saha et al. 1981). However, the significance of the effect is still unclear. Sandeep et al. (2018) pointed out that the sample size in Saha et al. (1981) might be too small. Hurley and Boos (2015) did not find a large number of MLPSs over the BoB to originate from the west Pacific.

The average lifetime is another important attribute of MLPSs that has not been discussed extensively in previous studies. A typical MLPS lasts about 3–6 days (Sikka 1977; Hurley and Boos 2015; Dong et al. 2017). The average lifetime in ERA-Interim is 5.1 days, and depressions (6.1 days) persist longer than lows (3.8 days). On average, MLPSs spend about half of their lifetime over ocean. These values are in broad agreement with the CM4.0 historical simulation, which yields an average lifetime of 4.7 days (5.3 days for depressions and 3.7 days for lows) and 58% of their lifetime over ocean (Table 1). In summary, CM4.0 shows considerable skills in simulating South Asian MLPSs during the historical period, lending credibility to the model-projected future changes.

b. *Projected changes in MLPSs*

The average occurrence frequency is 5.8 per season in the future simulation (2064–99), a 18% decrease from the historical simulation (1979–2014). Consistent with Sandeep et al. (2018), this reduction occurs mainly over

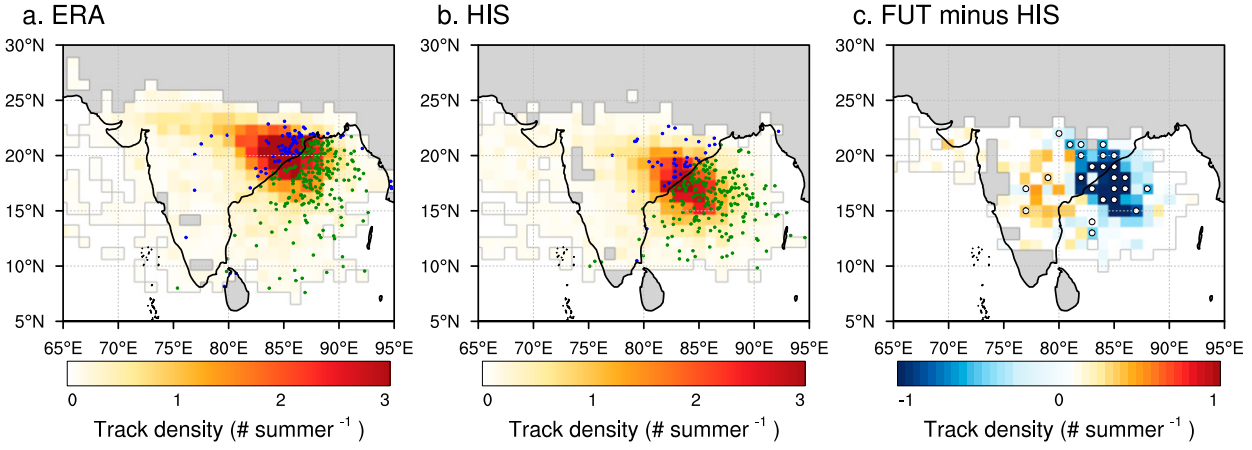

FIG. 1. Track density of MLPSs (number per season) based on (a) ERA-Interim and (b) the ensemble-mean historical simulations. Blue (green) dots in (a) and (b) denote the genesis locations over land (ocean). The dots in (b) are from one of the three simulations. (c) The difference between the future and historical simulations (the former minus the latter, as is the convention throughout the paper). White dots indicate changes that are statistically significant at the 95% confidence level. HIS and FUT refer to the historical and future simulations, respectively.

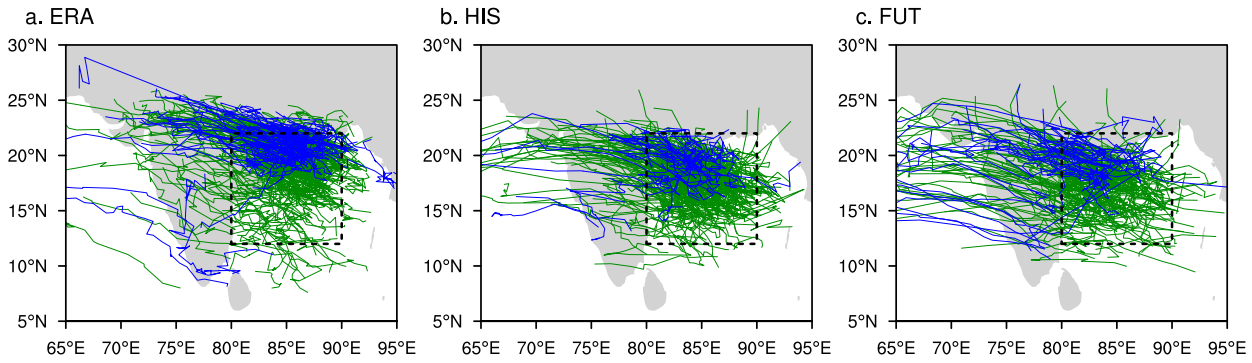

FIG. 2. Tracks of MLPSs based on (a) ERA-Interim, (b) one of the three historical simulations, and (c) the future simulation. Blue (green) lines denote the tracks of MLPSs generated over land (ocean). The black dashed rectangles mark the core MLPS genesis region.

ocean (−25%), with a smaller but robust increase in the number of MLPSs over land (7%). Both monsoon depressions and lows are less frequent under the warming scenario. The respective decreases are 18% and 19%. Interestingly, the average lifetime and typical tracks of MLPSs remain almost unchanged regardless of intensity or location (Table 1 and Fig. 2).

Compared with the historical simulation, there is a widespread reduction in track density over much of the core genesis region (Fig. 1; i.e., the northwestern portion of the BoB and the adjacent coastal regions as denoted by the rectangles in Fig. 2) while denser tracks are tightly clustered over the Indian subcontinent near 15°N. The latter point is particularly salient in Fig. 2—the number of tracks crossing the Indian subcontinent is visibly higher under the warming scenario. Despite the large regional changes in frequency, the mean genesis location remains almost the same (Table 1).

c. *Changes in the large-scale environment*

The environmental variables associated with MLPS formation may hold the key to understanding the projected changes in occurrence frequency. A number of prior studies have identified the dynamic and thermodynamic conditions favorable to MLPS genesis, with low-level (850-hPa) relative vorticity (ζ_{850}), vertical wind shear (V_s), midlevel (600-hPa) relative humidity (RH_{600}), and total column water vapor [or water vapor path (WVP)] highlighted as being particularly influential (Ditchek et al. 2016; Rastogi et al. 2018; Sandeep et al. 2018). SST and CAPE may also be relevant, as in tropical cyclogenesis (Tuleya et al. 2016).

The ability of CM4.0 to simulate the climatological seasonal means of the environmental variables is evaluated by comparing with reanalysis or observations in Figs. 3–8. The model-simulated low-level mean flow over the South Asian monsoon region bears a close resemblance to the reanalysis (Fig. 3). The monsoon trough (characteristic of large positive 850-hPa relative vorticity at ζ_{850}), however, is deeper than in ERA-Interim, and its center is shifted slightly southward. This is consistent with the simulated MLPS genesis being south of ERA-Interim (Fig. 1). The vertical wind shear is relatively strong over the Arabian Sea and the BoB, acting to limit the intensification of synoptic-scale disturbances into tropical cyclones (Vishnu et al. 2016; Hunt and Turner 2017). The model captures the distribution pattern of vertical wind shear fairly well. It simulates the strong shear over the Arabian Sea and the southern BoB with slight overestimation (Fig. 4).

CM4.0 captures the spatial structure of WVP, but underestimates its magnitude over most of the domain (Fig. 5). The 600-hPa relative humidity is appreciably lower over the core genesis region and much of the subcontinent in the model than in the reanalysis, which presumably has a suppressing effect on moist convection and MLPSs. The model also places the maximum RH_{600} south of the reanalysis (Fig. 6). While the distribution of SST over the Arabian Sea is sufficiently similar between the observations and model simulation, the model fails to capture the relatively warm SSTs in the BoB, especially along the east coast of India (Fig. 7). Despite an overall overestimate, the simulated spatial pattern of CAPE is generally in good agreement with ERA-Interim, with a distinct maximum over the BoB (Fig. 8).

We further analyze the same set of environmental variables composited on MLPS genesis, referred to as event-based analysis hereinafter. Table 2 lists the seasonal mean variables averaged over the MLPS core genesis region and event-based variables averaged over all MLPS events. A comparison of these metrics suggests that MLPSs tend to form at ζ_{850} values much higher than the seasonal mean. Higher WVP, midlevel relative humidity, and convective instability are also favorable to MLPS formation. The other variables examined here show no significant difference between the

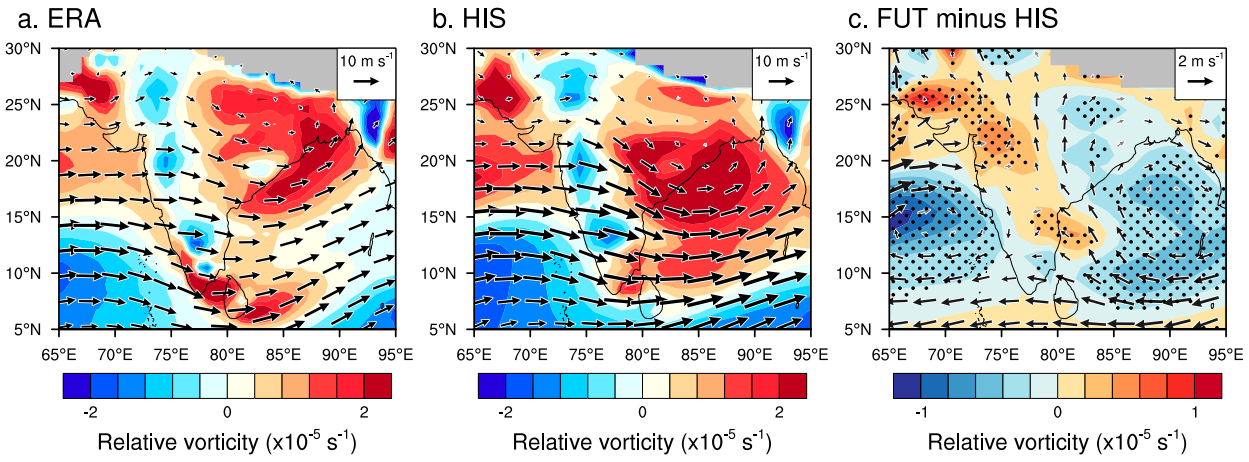

FIG. 3. Seasonal mean low-level (850-hPa) relative vorticity (10^{-5} s^{-1}) overlaid with 850-hPa wind vectors (m s^{-1}) based on (a) ERA-Interim and (b) the ensemble-mean historical simulations. (c) The difference between the future and historical simulations. Stippling and black arrows indicate changes that are statistically significant at the 95% confidence. Gray shading indicates where the pressure level is below the surface.

seasonal mean and event-based values. These results are consistent with the previous finding that precipitating vortices are more likely to develop in a warm, moist, convectively unstable environment with high ambient vorticity (Sikka 1977; Prajeesh et al. 2013), and lend further support to the study by Ditchek et al. (2016), which used a statistical model to infer that lower tropospheric vorticity and atmospheric moisture content are the main contributing factors to MLPS genesis. Event-based results from the historical simulation reaffirm the critical role of ζ_{850} in MLPS formation, while underestimating those of atmospheric moisture and stability.

The question then becomes how these environmental variables would change in the future simulation, and what is the implication for MLPS formation. CM4.0 simulates a notable reduction in ζ_{850} over much of the core genesis region, indicating that the circulation becomes more anticyclonic (Fig. 3). This is accompanied by an increase over the western part of the subcontinent. Given the link between background vorticity and MLPS formation, it is not surprising to see that the spatial patterns of the changes in ζ_{850} are broadly consistent with those of the changes in MLPS number density (Fig. 1) and tracks (Fig. 2). This indicates that the overall decrease in MLPS number can be attributed, at least in part, to the reduction in lower-tropospheric vorticity over the core MLPS genesis region.

Although the seasonal mean ζ_{850} over the core genesis region declines by 10%, the event-based ζ_{850} increases by 9% (Table 2). In other words, it takes even higher vorticity for MLPSs to form in the future simulation.

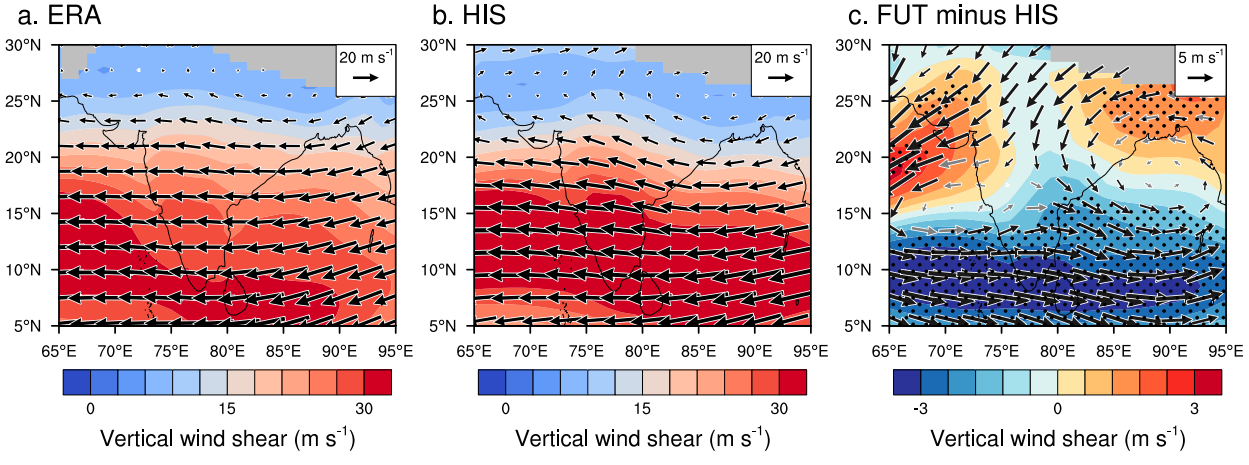

FIG. 4. As in Fig. 3, but for vertical wind shear (m s^{-1}).

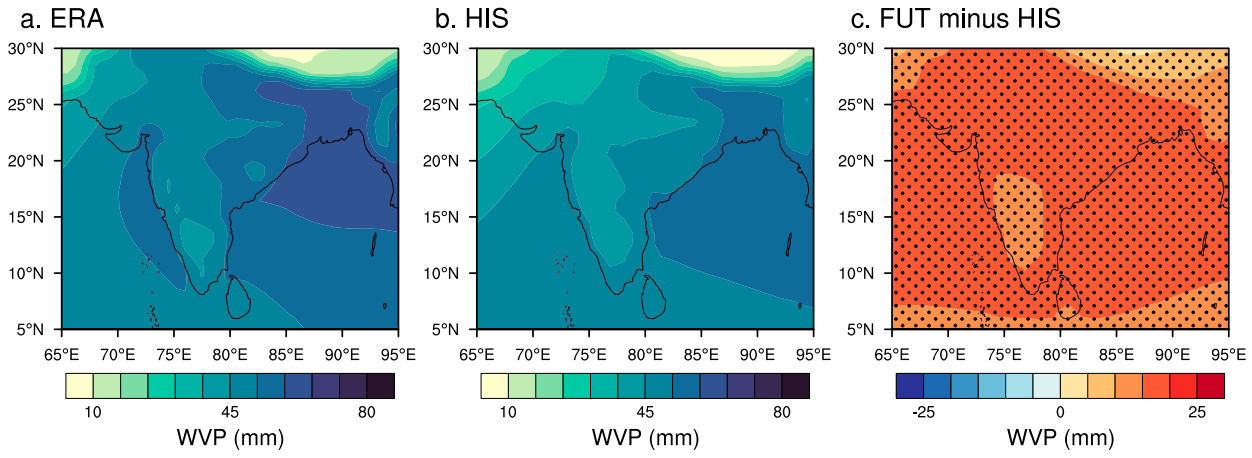

FIG. 5. As in Fig. 3, but for WVP (mm).

Since the frequency (or probability) of these vorticities high enough for MLPS formation scales approximately with the mean (not shown), a decrease in seasonal mean vorticity would translate into a reduction in MLPS number. It is also worth noting that ζ_{850} decreases sharply over the southern Arabian Sea, suggesting that the local cyclonic vortex genesis may become less common under warming (Murakami et al. 2013).

CM4.0 simulates a reduction in V_s over much of the Arabian Sea and the BoB (Fig. 4), which amounts to 4% over the core genesis region (Table 2). WVP increases substantially everywhere (Fig. 5), with an average fractional change of 30% over the core genesis region (Table 2). On the other hand, RH_{600} remains almost unchanged over ocean (Fig. 6), while SST increases by almost 3 K (Fig. 7). This helps explain why WVP roughly scales with SST following the Clausius–Clapeyron relation. Warmer and wetter lower tropospheric conditions make the atmospheric column more convectively unstable (Fig. 8). All of these changes, however, would create a more favorable environment for MLPS formation. This reasoning indicates that the aforementioned reduction in ζ_{850} may be the sole factor responsible for the simulated reduction in MLPS number.

A major source of vorticity is the stretching term in the vorticity equation, which is proportional to large-scale divergence or vertical velocity ω (Sardeshmukh and Held 1984). As shown in Fig. 9, the change in 850-hPa ω has a spatial pattern similar to the seasonal mean, but of the opposite sign, suggesting a slowdown of the large-scale circulation. There is a widespread weakening of the climatological ascending motion over the BoB. More specifically, ω_{850} decreases by 21% over the core genesis region, which must be at least partly responsible for the reduction in ζ_{850} through the vorticity stretching term. Since precipitation can be approximated as the product of large-scale ascent at the boundary layer top and boundary layer moisture (i.e., $P \sim \omega \times$ WVP), the

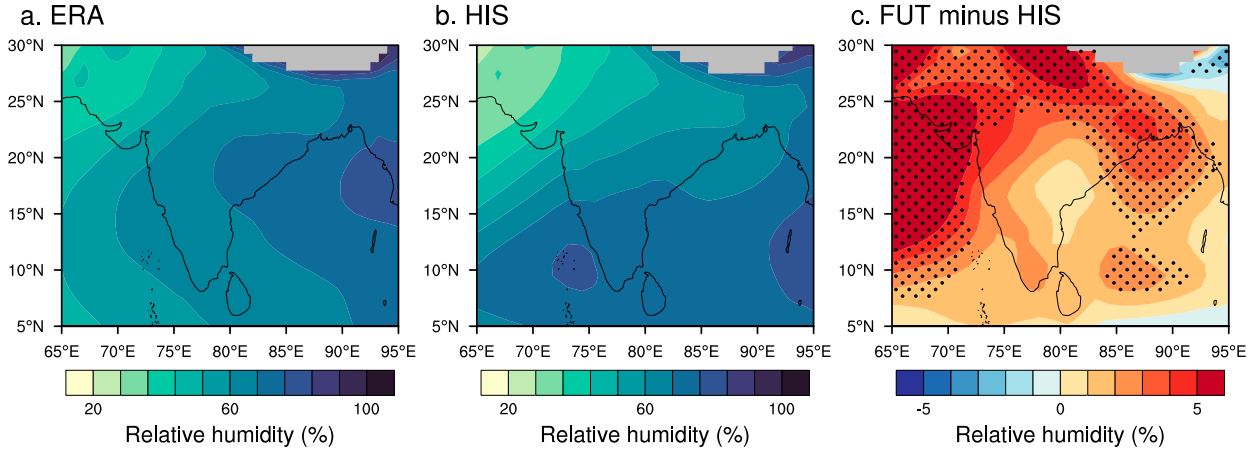

FIG. 6. As in Fig. 3, but for midlevel (600-hPa) relative humidity (%).

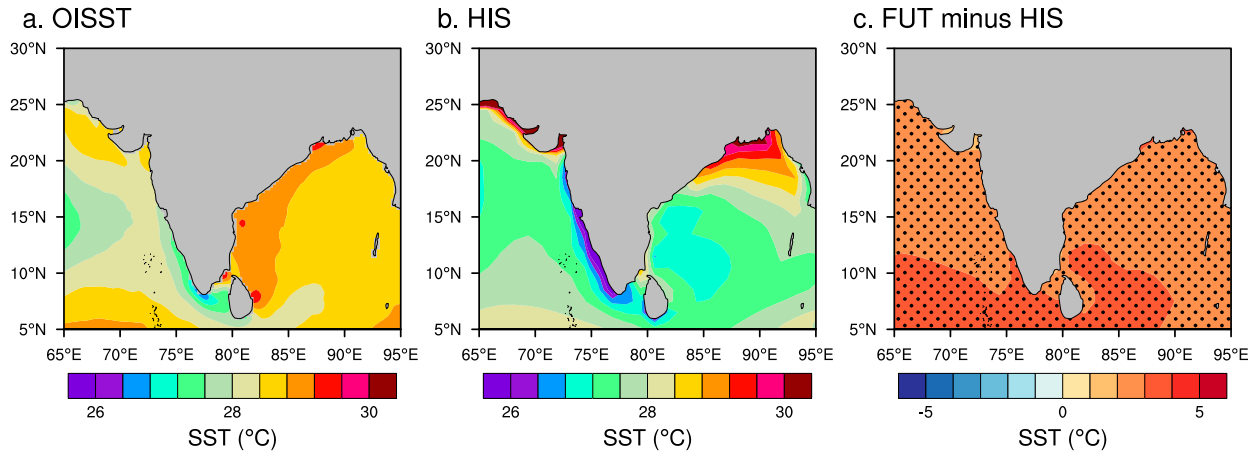

FIG. 7. As in Fig. 3, but for sea surface temperature (°C); (a) is based on the NOAA High-Resolution Blended Analysis of Daily SST.

fraction change in precipitation ($\Delta P/P$) can be written as $\Delta\omega/\omega$ + ΔWVP/WVP. Thus, one can decompose the fractional change in ω_{850} into those in precipitation (+10%) and WVP (−30%). Although the argument that the global-mean precipitation, which is controlled tightly by the atmospheric radiative balance, cannot increase as fast as water vapor (the Clausius–Clapeyron relation) (Held and Soden 2006) is not strictly applicable to a specific region, the above changes over the core genesis region can be thought of as a local manifestation of the same physical mechanism.

A point that needs clarification is that the aforementioned seasonal mean environmental variables (ζ_{850} in particular) include the contributions from MLPSs, and strictly speaking, do not represent the background felt by MLPSs in a clean way. A rough estimate based on the assumption that MLPSs remain within the core genesis region through their lifetime suggests that the probability of a grid point in the region encountering a MLPS at any given time during the monsoon season is only about 0.3%. Also, if one contrasts the historical and future simulations, the seasonal mean ζ_{850} decreases by 10% while the event-based ζ_{850} increases by 9% (Table 2). If the former is dominated by MLPSs, it would increase as is the case for the latter. This is why we believe that MLPSs do not contribute significantly to the large-scale environmental variables.

d. *Potential impacts on precipitation*

Any change in the occurrence frequency of MLPSs can also alter the associated precipitation. The model-simulated total monsoon precipitation compares well

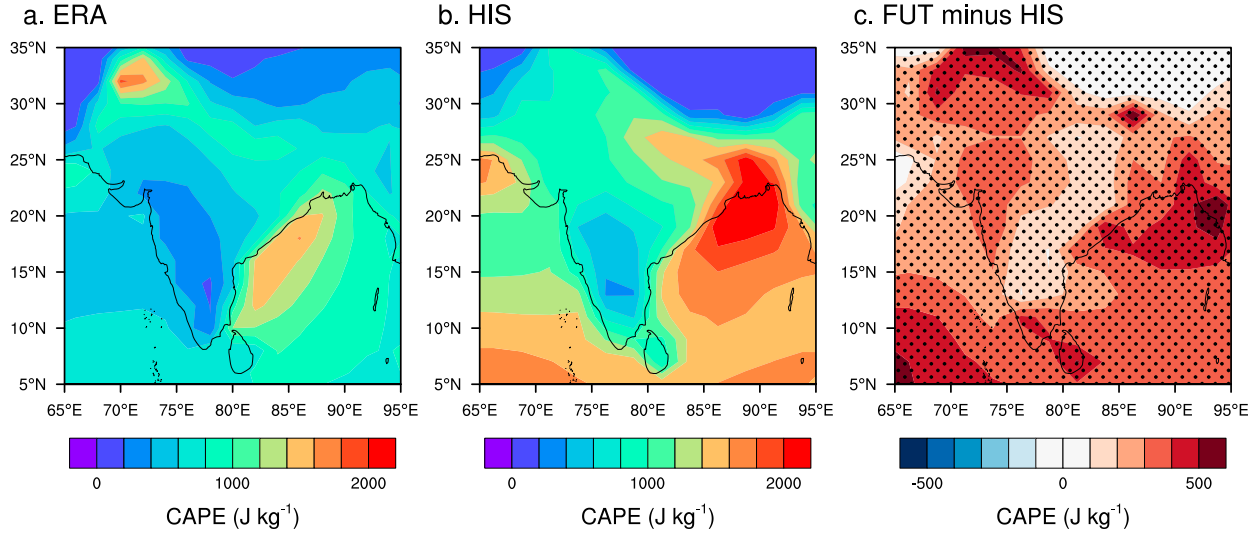

FIG. 8. As in Fig. 3, but for CAPE (J kg^{-1}).

TABLE 2. Seasonal mean and event-based large-scale environmental variables relevant to MLPS formation in the ERA-Interim and historical simulation and the differences between the historical and future simulations (with statistical significance at the 95% confidence level highlighted in boldface). Note that the seasonal means are over the core genesis region.

	ERA-Interim		Historical simulation		Future minus historical	
Variable	Mean	Event-based	Mean	Event-based	Mean	Event-based
ζ_{850} (10^{-5} s^{-1})	1.1	4.5	2.1	5.3	**−0.2**	0.5
V_s (m s^{-1})	23.3	19.8	23.3	26.5	−0.9	−1.3
WVP (mm)	58.1	66.0	53.0	52.3	**16.0**	**12.6**
RH_{600} (%)	70.9	83.8	67.6	68.3	2.0	0.2
SST (°C)	28.8	28.7	27.6	28.3	**2.8**	**2.1**
CAPE (J kg^{-1})	1065.1	1080.0	1618.8	1576.1	**327.2**	**243.6**

with the GPCP dataset in terms of spatial distribution, with maxima centered over the northeastern BoB, Western Ghats, and north-central India (Fig. 10). But the model overestimates orographic precipitation near the southern foothill of the Himalayas. This excess of orographic precipitation is consistent with the low-level westerlies being too strong in the model (Fig. 3). Moreover, the center of precipitation over north-central India is shifted toward the south of the observations by a few degrees of latitude, which is consistent with the bias in MLPS track density (Fig. 1).

A few methods have been used to associate precipitation with the occurrence of MLPSs. In this study we assume a radius of influence around each MLPS, and attribute all precipitation occurring within this radius to that system. This method has been shown to be more reliable than considering all rainfall on each MLPS day (e.g., Rastogi et al. 2018; Sandeep et al. 2018), and, despite its simplicity, provides comparable estimates to much more complicated clustering analyses (Hunt and Fletcher 2019).

As the typical horizontal scale of MLPSs is about 2000 km (Ding and Sikka 2006; Cohen and Boos 2014; Hurley and Boos 2015; Ditchek et al. 2016; Hunt et al. 2016b), we choose a fixed radius of influence of 1000 km. This yields an estimate of the fraction of MLPS-related precipitation at around 50% in the core monsoon region for GPCP (Fig. 11). Although the value is somewhat lower than in previous studies using other attribution methods, the spatial distribution is similar (Dong et al. 2017; Hunt and Fletcher 2019). The low bias may arise from the use of daily records here, as coarse temporal resolutions tend to smooth out the precipitation maxima associated with MLPSs. The historical simulation captures the spatial pattern rather well, but underestimates the contribution of MLPSs (Fig. 11). This may be related to the tropospheric moisture content in CM4.0 being biased low (Fig. 5). We probe the robustness of the results using other values for the radius of influence (800 and 1200 km). The MLPS-related contributions vary in tandem with radius, but the overall patterns are similar (Fig. 11).

The future simulation shows substantial increases in the total monsoon precipitation along the Western Ghats, over the western BoB, and in the eastern Himalayan region (Fig. 10). These results are consistent with many

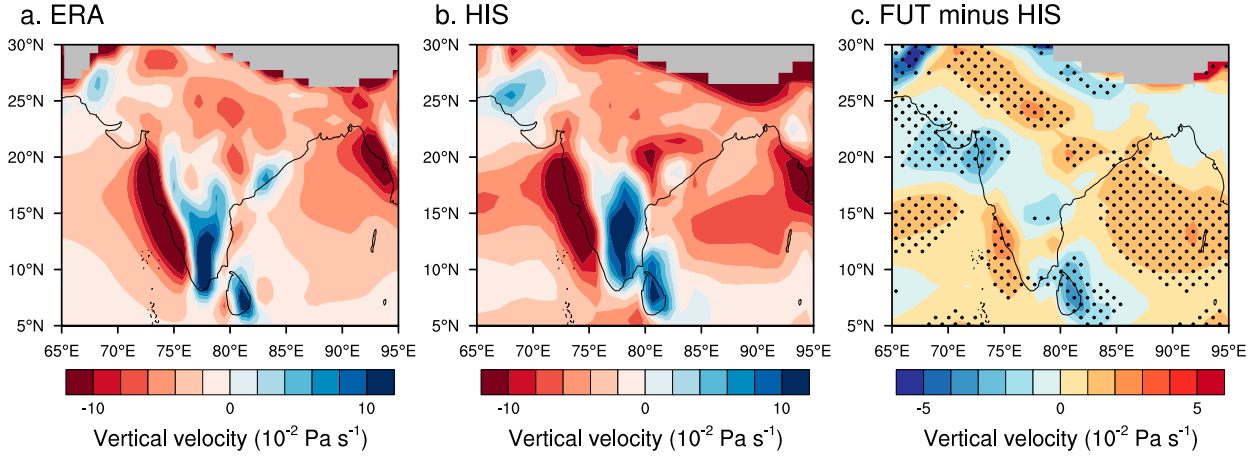

FIG. 9. As in Fig. 3, but for 850-hPa vertical velocity (10^{-2} Pa s^{-1}).

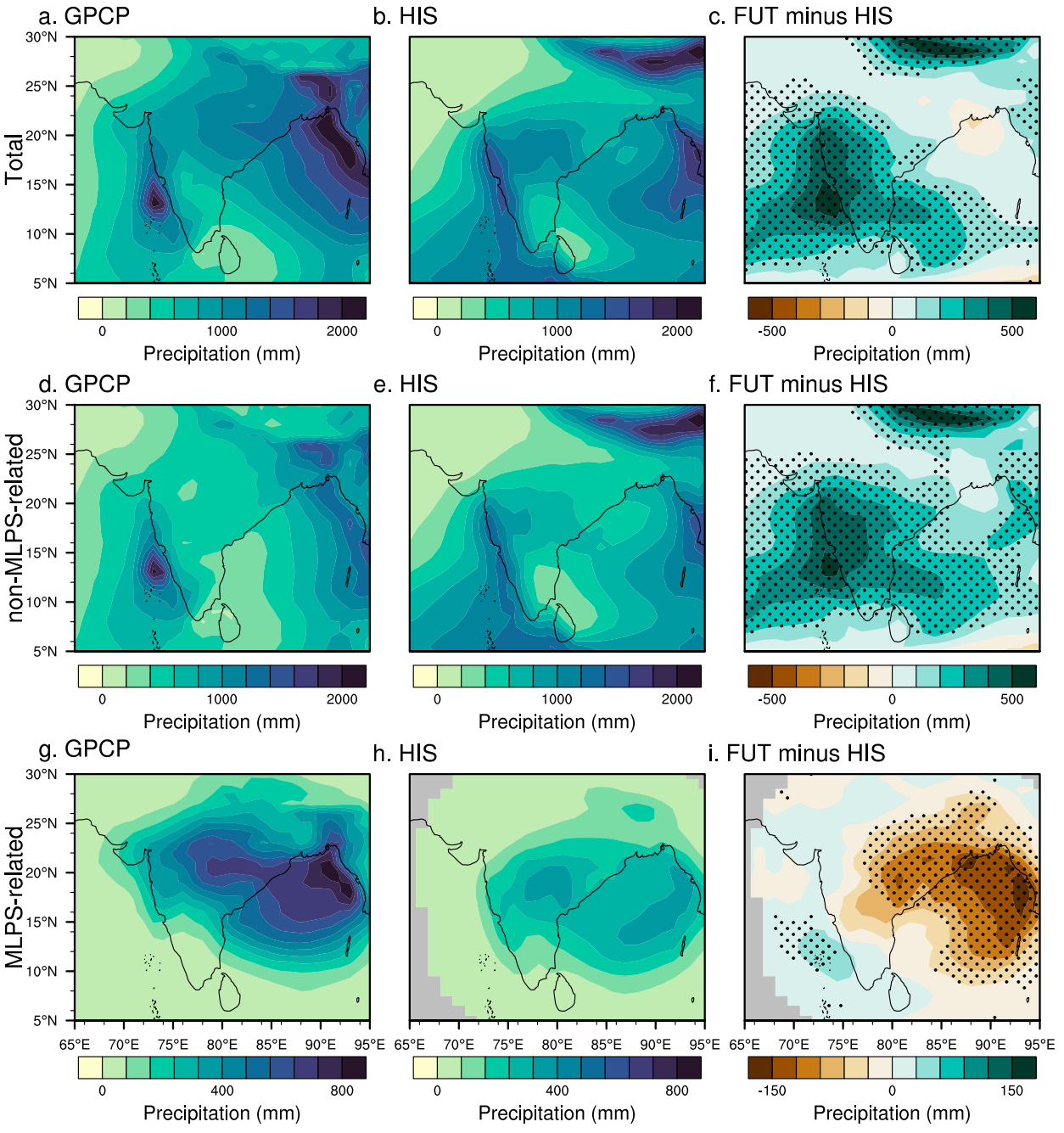

FIG. 10. Seasonal total precipitation (mm per season) based on (a) GPCP and (b) the ensemble-mean historical simulations. (c) The difference between the future and historical simulations. (d)–(f) As in (a)–(c), but for non-MLPS-related precipitation. (g)–(i) As in (a)–(c), but for MLPS-related precipitation. Stippling in (c), (f), and (i) indicates changes that are statistically significant at the 95% confidence level. Gray shading indicates where no MLPS-related precipitation is present.

previous studies, which have attributed the increase in mean precipitation primarily to atmospheric moistening as climate warms (Stowasser et al. 2009; Turner and Annamalai 2012; Rastogi et al. 2018). Interestingly, the core MLPS genesis region experiences very small increases in precipitation, or even reductions relative to the historical simulation. Unlike the seasonal mean, MLPS-related precipitation shows significant decreases stretching westward from the core MLPS genesis region into central India (Fig. 10), mirroring the simulated decrease in MLPS number (Fig. 1). This explains why the total precipitation response over the core MLPS genesis

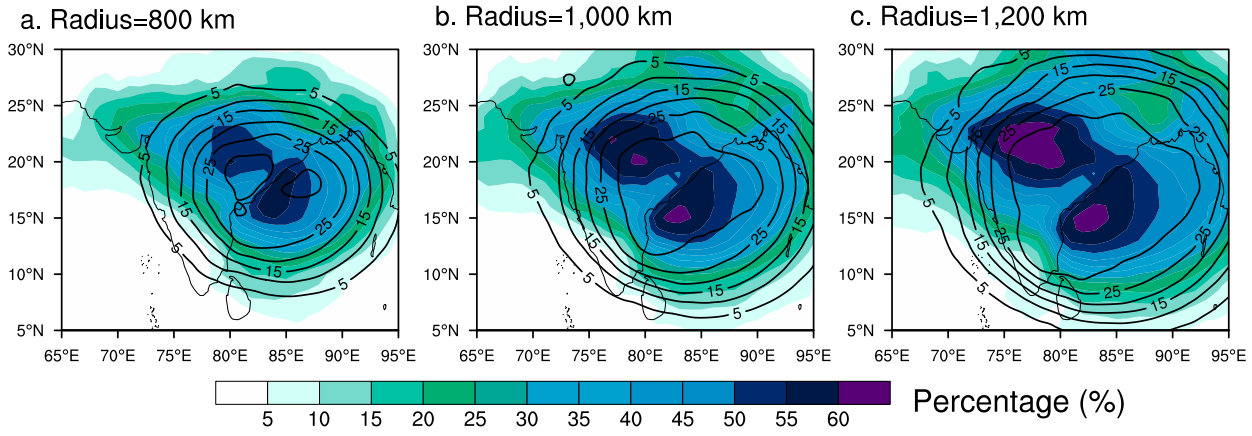

FIG. 11. Contribution of MLPS-related precipitation to the total seasonal precipitation (%) with the radius of influence at (a) 800, (b) 1000, and (c) 1200 km based on GPCP (shading) and the ensemble-mean historical simulations (contours).

region, most notably north-central India, is different from the rest of the South Asian monsoon region. By contrast, a significant increase in MLPS-related precipitation is found over the Arabian Sea. This can be linked to denser MLPS tracks in this region (Fig. 2), along with increased atmospheric moisture (Fig. 5). A significant increase in MLPS-related precipitation is also seen for the foothill of the Himalayas. On the other hand, non-MLPS-related precipitation undergoes a much more uniform increase over the entire monsoon region, which is presumably caused by the widespread increase in WVP (Fig. 5). It is interesting that the future South Asian monsoon precipitation increases simulated by CMIP3 and CMIP5 models are rather evenly distributed (Turner and Annamalai 2012; Sooraj et al. 2015), bearing more resemblance to CM4.0's non-MLPS-related precipitation increase than the MLPS-related precipitation decrease. The main reason is that CMIP models are not as skillful at simulating MLPSs as CM4.0, highlighting the importance of realistic representation of MLPSs in GCMs for projecting future South Asian monsoon precipitation change.

4. Conclusions

Confidence in model projections of future changes in MLPS activity is contingent on models' ability to simulate MLPSs in the current climate. We show that the GFDL CM4.0 model is skillful at simulating the key characteristics of these synoptic systems. In this sense, future projections based on CM4.0 may be particularly relevant to assessing potential changes in monsoon climate.

CM4.0 projects a significant decrease in MLPS number over the South Asian monsoon region. We further analyze the large-scale environmental variables to better understand the underlying mechanism of this decrease in MLPS activity, and find that a reduction in low-level relative vorticity over the core MLPS genesis region is the primary contributing factor. This reduction in MLPS occurrence has significant impacts on monsoon precipitation. Despite increases in the total precipitation across much of the monsoon region, CM4.0 simulates little change or even slight decreases in precipitation over the core MLPS genesis region. This change is consistent with a significant decrease in MLPS-related precipitation that stretches westward from the core genesis region into the north-central India. As extreme precipitation events are closely linked to MLPS activity over that region (Dong et al. 2018), our results may have important implications for the vulnerable areas both within and along the margins of the monsoon region.

Acknowledgments. The authors thank Yanluan Lin, Jonathon Wright, Steve Garner, and Spencer Clark for their helpful comments on earlier versions of this paper. This research from the Geophysical Fluid Dynamics Laboratory is supported by NOAA's Science Collaboration Program and administered by UCAR's Cooperative Programs for the Advancement of Earth System Science (CPAESS) under Awards NA16NWS4620043 and NA18NWS4620043B.

REFERENCES

Adames, A. F., and Y. Ming, 2018a: Moisture and moist static energy budgets of South Asian monsoon low pressure systems in GFDL AM4.0. *J. Atmos. Sci.*, **75**, 2107–2123, https://doi.org/10.1175/JAS-D-17-0309.1.

——, and ——, 2018b: Interactions between water vapor and potential vorticity in synoptic-scale monsoonal disturbances: Moisture vortex instability. *J. Atmos. Sci.*, **75**, 2083–2106, https://doi.org/10.1175/JAS-D-17-0310.1.

Adcroft, A., and Coauthors, 2019: The GFDL Global Ocean and Sea Ice Model OM4.0: Model description and simulation features. *J. Adv. Model. Earth Syst.*, **11**, 3167–3211, https://doi.org/10.1029/2019MS001726.

Ajayamohan, R. S., W. J. Merryfield, and V. V. Kharin, 2010: Increasing trend of synoptic activity and its relationship with extreme rain events over central India. *J. Climate*, **23**, 1004–1013, https://doi.org/10.1175/2009JCLI2918.1.

Clark, S. K., Y. Ming, and A. F. Adames, 2020: Monsoon low pressure system like variability in an idealized moist model. *J. Climate*, **33**, 2051–2074, https://doi.org/10.1175/JCLI-D-19-0289.1.

Cohen, N. Y., and W. R. Boos, 2014: Has the number of Indian summer monsoon depressions decreased over the last 30 years? *Geophys. Res. Lett.*, **41**, 7846–7853, https://doi.org/10.1002/2014GL061895.

Dee, D. P., and Coauthors, 2011: The ERA-Interim reanalysis: Configuration and performance of the data assimilation system. *Quart. J. Roy. Meteor. Soc.*, **137**, 553–597, https://doi.org/10.1002/qj.828.

Ding, Y., and D. R. Sikka, 2006: Synoptic systems and weather. *The Asian Monsoon*, Springer, 131–201.

Ditchek, S. D., W. R. Boos, S. J. Camargo, and M. K. Tippett, 2016: A genesis index for monsoon disturbances. *J. Climate*, **29**, 5189–5203, https://doi.org/10.1175/JCLI-D-15-0704.1.

Dong, W. H., Y. L. Lin, J. S. Wright, Y. Y. Xie, F. H. Xu, W. Q. Xu, and Y. Wang, 2017: Indian monsoon low-pressure systems feed up-and-over moisture transport to the southwestern Tibetan Plateau. *J. Geophys. Res. Atmos.*, **122**, 12 140–12 151, https://doi.org/10.1002/2017JD027296.

——, and Coauthors, 2018: Connections between a late summer snowstorm over the southwestern Tibetan Plateau and a concurrent Indian monsoon low-pressure system. *J. Geophys. Res. Atmos.*, **123**, 13 676–13 691, https://doi.org/10.1029/2018JD029710.

Held, I. M., and B. J. Soden, 2006: Robust responses of the hydrological cycle to global warming. *J. Climate*, **19**, 5686–5699, https://doi.org/10.1175/JCLI3990.1.

——, and Coauthors, 2019: Structure and performance of GFDL's CM4.0 climate model. *J. Adv. Model. Earth Syst.*, **11**, 3691–3727, https://doi.org/10.1029/2019MS001829.

Huffman, G. J., R. F. Adler, M. M. Morrissey, D. T. Bolvin, S. Curtis, R. Joyce, B. McGavock, and J. Susskind, 2001: Global precipitation at one-degree daily resolution from multisatellite observations. *J. Hydrometeor.*, **2**, 36–50, https://doi.org/10.1175/1525-7541(2001)002<0036:GPAODD>2.0.CO;2.

Hunt, K. M. R., and A. G. Turner, 2017: The effect of horizontal resolution on Indian monsoon depressions in the Met Office NWP model. *Quart. J. Roy. Meteor. Soc.*, **143**, 1756–1771, https://doi.org/10.1002/qj.3030.

——, and J. K. Fletcher, 2019: The relationship between Indian monsoon rainfall and low-pressure systems. *Climate Dyn.*, **53**, 1859–1871, https://doi.org/10.1007/s00382-019-04744-x.

——, A. G. Turner, P. M. Inness, D. E. Parker, and R. C. Levine, 2016a: On the structure and dynamics of Indian monsoon depressions. *Mon. Wea. Rev.*, **144**, 3391–3416, https://doi.org/10.1175/MWR-D-15-0138.1.

——, ——, and D. E. Parker, 2016b: The spatiotemporal structure of precipitation in Indian monsoon depressions. *Quart. J. Roy. Meteor. Soc.*, **142**, 3195–3210, https://doi.org/10.1002/qj.2901.

Hurley, J. V., and W. R. Boos, 2015: A global climatology of monsoon low-pressure systems. *Quart. J. Roy. Meteor. Soc.*, **141**, 1049–1064, https://doi.org/10.1002/qj.2447.

Jayanthi, N., M. Rajeevan, A. Srivastava, D. Sunita, S. K. Roy Bhowmik, and H. Hatwar, 2006: Monsoon 2006: A report. IMD Meteorology Monograph/Synoptic Meteorology 4/2006, 103 pp.

Krishnamurthy, V., and R. S. Ajayamohan, 2010: Composite structure of monsoon low pressure systems and its relation to Indian rainfall. *J. Climate*, **23**, 4285–4305, https://doi.org/10.1175/2010JCLI2953.1.

Krishnamurti, T., J. Molinari, H. Pan, and V. Wong, 1977: Downstream amplification and formation of monsoon disturbances. *Mon. Wea. Rev.*, **105**, 1281–1297, https://doi.org/10.1175/1520-0493(1977)105<1281:DAAFOM>2.0.CO;2.

Krishnan, R., D. C. Ayantika, V. Kumar, and S. Pokhrel, 2011: The long-lived monsoon depressions of 2006 and their linkage with the Indian Ocean Dipole. *Int. J. Climatol.*, **31**, 1334–1352, https://doi.org/10.1002/joc.2156.

Lau, N. C., and M. J. Nath, 2003: Atmosphere–ocean variations in the Indo-Pacific sector during ENSO episodes. *J. Climate*, **16**, 3–20, https://doi.org/10.1175/1520-0442(2003)016<0003:AOVITI>2.0.CO;2.

Mooley, D. A., and J. Shukla, 1988: Characteristics of the westward-moving summer monsoon low pressure systems over the Indian region and their relationship with the monsoon rainfall. University of Maryland, Center for Ocean–Land–Atmosphere Interactions, 47 pp.

Murakami, H., M. Sugi, and A. Kitoh, 2013: Future changes in tropical cyclone activity in the North Indian Ocean projected by high-resolution MRI-AGCMs. *Climate Dyn.*, **40**, 1949–1968, https://doi.org/10.1007/s00382-012-1407-z.

O'Neill, B. C., and Coauthors, 2016: The Scenario Model Intercomparison Project (ScenarioMIP) for CMIP6. *Geosci. Model Dev.*, **9**, 3461–3482, https://doi.org/10.5194/gmd-9-3461-2016.

Prajeesh, A. G., K. Ashok, and D. V. B. Rao, 2013: Falling monsoon depression frequency: A Gray-Sikka conditions perspective. *Sci. Rep.*, **3**, 2989, https://doi.org/10.1038/SREP02989.

Praveen, V., S. Sandeep, and R. S. Ajayamohan, 2015: On the relationship between mean monsoon precipitation and low pressure systems in climate model simulations. *J. Climate*, **28**, 5305–5324, https://doi.org/10.1175/JCLI-D-14-00415.1.

Rastogi, D., M. Ashfaq, L. R. Leung, S. Ghosh, A. Saha, K. Hodges, and K. Evans, 2018: Characteristics of Bay of Bengal monsoon depressions in the 21st century. *Geophys. Res. Lett.*, **45**, 6637–6645, https://doi.org/10.1029/2018GL078756.

Reynolds, R. W., T. M. Smith, C. Liu, D. B. Chelton, K. S. Casey, and M. G. Schlax, 2007: Daily high-resolution-blended analyses for sea surface temperature. *J. Climate*, **20**, 5473–5496, https://doi.org/10.1175/2007JCLI1824.1.

Saha, K., F. Sanders, and J. Shukla, 1981: Westward propagating predecessors of monsoon depressions. *Mon. Wea. Rev.*, **109**, 330–343, https://doi.org/10.1175/1520-0493(1981)109<0330:WPPOMD>2.0.CO;2.

Sandeep, S., R. S. Ajayamohan, W. R. Boos, T. P. Sabin, and V. Praveen, 2018: Decline and poleward shift in Indian summer monsoon synoptic activity in a warming climate. *Proc. Natl. Acad. Sci. USA*, **115**, 2681–2686, https://doi.org/10.1073/pnas.1709031115.

Sardeshmukh, P. D., and I. M. Held, 1984: The vorticity balance in the tropical upper troposphere of a general circulation model. *J. Atmos. Sci.*, **41**, 768–778, https://doi.org/10.1175/1520-0469(1984)041<0768:TVBITT>2.0.CO;2.

Sikka, D. R., 1977: Some aspects of the life history, structure and movement of monsoon depressions. *Pure Appl. Geophys.*, **115**, 1501–1529, https://doi.org/10.1007/BF00874421.

——, 2006: *A Study on the Monsoon Low Pressure Systems over the Indian Region and Their Relationship with Drought and*

Excess Monsoon Seasonal Rainfall. Center for Ocean–Land–Atmosphere Studies, Center for the Application of Research on the Environment, 61 pp.

Sooraj, K. P., P. Terray, and M. Mujumdar, 2015: Global warming and the weakening of the Asian summer monsoon circulation: assessments from the CMIP5 models. *Climate Dyn.*, **45**, 233–252, https://doi.org/10.1007/s00382-014-2257-7.

Stowasser, M., H. Annamalai, and J. Hafner, 2009: Response of the South Asian summer monsoon to global warming: Mean and synoptic systems. *J. Climate*, **22**, 1014–1036, https://doi.org/10.1175/2008JCLI2218.1.

Tuleya, R. E., M. Bender, T. R. Knutson, J. J. Sirutis, B. Thomas, and I. Ginis, 2016: Impact of upper-tropospheric temperature anomalies and vertical wind shear on tropical cyclone evolution using an idealized version of the operational GFDL hurricane model. *J. Atmos. Sci.*, **73**, 3803–3820, https://doi.org/10.1175/JAS-D-16-0045.1.

Turner, A. G., and H. Annamalai, 2012: Climate change and the South Asian summer monsoon. *Nat. Climate Change*, **2**, 587–595, https://doi.org/10.1038/nclimate1495.

Vishnu, S., P. A. Francis, S. S. C. Shenoi, and S. S. V. S. Ramakrishna, 2016: On the decreasing trend of the number of monsoon depressions in the Bay of Bengal. *Environ. Res. Lett.*, **11**, 014011, https://doi.org/10.1088/1748-9326/11/1/014011.

Wilks, D. S., 2016: "The stippling shows statistically significant grid points": How research results are routinely overstated and overinterpreted, and what to do about it. *Bull. Amer. Meteor. Soc.*, **97**, 2263–2273, https://doi.org/10.1175/BAMS-D-15-00267.1.

Yoon, J.-H., and W.-R. Huang, 2012: Indian monsoon depression: Climatology and variability. *Modern Climatology*, S.-Y. Wang, Ed., InTech, 45–72.

Zhao, M., I. M. Held, S. J. Lin, and G. A. Vecchi, 2009: Simulations of global hurricane climatology, interannual variability, and response to global warming using a 50-km resolution GCM. *J. Climate*, **22**, 6653–6678, https://doi.org/10.1175/2009JCLI3049.1.

——, and Coauthors, 2018a: The GFDL global atmosphere and land model AM4.0/LM4.0:1. Simulation characteristics with prescribed SSTs. *J. Adv. Model. Earth Syst.*, **10**, 691–734, https://doi.org/10.1002/2017MS001208.

——, and Coauthors, 2018b: The GFDL global atmosphere and land model AM4.0/LM4.0:2. Model description, sensitivity studies, and tuning strategies. *J. Adv. Model. Earth Syst.*, **10**, 735–769, https://doi.org/10.1002/2017MS001209.